Nanoscale Horizons

ROYAL SOCIETY OF CHEMISTRY

COMMUNICATION

View Article Online
View Journal | View Issue

Check for updates

Cite this: *Nanoscale Horiz.*, 2025, **10**, 2584

Received 20th May 2025,
Accepted 30th July 2025

DOI: 10.1039/d5nh00357a

rsc.li/nanoscale-horizons

Published on 13 August 2025. Downloaded on 2/14/2026 1:29:38 AM.

A long-staple design approach towards the scalable production of scaffolded DNA origami

Chanseok Lee, *[a] Yanggyun Kim, †[b] Kyounghwa Jeon, [b] Taeyoung Ryu [b] and Do-Nyun Kim *[bcd]

Scaffolded DNA origami enables the programmable construction of nanoscale structures through the hybridization of a long single-stranded scaffold with hundreds of short staple strands. However, the reliance on numerous synthetic oligonucleotides remains a key barrier to scalable and cost-effective production of DNA nanostructures. In this study, we introduce a long-staple design strategy that extends the length of individual staple strands to 100–200 nucleotides (nt), thereby reducing the total number of strands required while maintaining assembly efficiency and structural fidelity. We demonstrate that this approach is broadly compatible with a variety of origami architectures, including both manually designed lattice-based structures and algorithmically generated wireframe geometries, without requiring changes to well-established design workflows. Using representative 2D and 3D structures, we show that long staples can assemble efficiently under the same thermal annealing conditions and Mg^{2+} concentrations as short staples, yielding final structures with comparable morphology. To further support biological production of staple strands, we generated long staples *via* rolling circle amplification (RCA) using custom-designed circular templates, each encoding a specific long staple sequence. This modular design allows for flexible and selective synthesis of desired staples, either individually or in pooled formats. These RCA-derived staples were successfully used in structure assembly, confirming the feasibility of enzyme-based synthesis for long-staple designs. This modular and adaptable strategy offers a practical route toward scalable fabrication of functional DNA nanostructures across diverse design frameworks.

New concepts

This study introduces a long-staple design strategy for scaffolded DNA origami that significantly improves its compatibility with enzymatic DNA production methods, particularly rolling circle amplification (RCA). By extending the length of staple strands from 20–50 nt to 100–200 nt, the total number of oligonucleotides required for assembly is reduced, enabling modular and scalable production of DNA nanostructures. Each long staple can be enzymatically synthesized from a unique circular template, offering modularity and scalability—overcoming the limitations of traditional small-scale solid-phase synthesis. This method preserves full compatibility with widely adopted design pipelines for scaffolded DNA origami, including both manually designed lattice structures and algorithmically generated wireframe geometries. Across all tested architectures including planar, bundled, and wireframe shapes, we demonstrated that long-staple designs maintain equivalent folding behavior and structural integrity compared to conventional short-staple systems. This advancement provides new insight into how structural DNA nanotechnology can evolve toward cost-effective manufacturing. The framework also opens opportunities in materials science for the development of functional nanostructures that leverage enzymatic synthesis and base-level chemical modifications, paving the way for practical applications in sensing, therapeutics, and programmable materials.

Introduction

Over the past decades, the field of structural DNA nanotechnology has witnessed extensive progress in the development of structural design[1–4] and analytical tools[5–8] aimed at creating complex and sophisticated nanoscale assemblies—many of which are inaccessible through conventional top-down nanofabrication techniques.[9,10] These advances have also led to multidisciplinary applications in materials science, biotechnology, and medicine, where DNA-based nanostructures serve as customizable platforms for molecular positioning,[11–13] sensing,[14,15] and therapeutical delivery.[16–19]

Among a variety of design methods, scaffolded DNA origami offers versatile shape design by folding a long single-stranded DNA scaffold with the aid of hundreds of short synthetic oligonucleotides, thereby enabling the formation of complex, programmable shapes with high fidelity.[3] It has become a widely adopted and standardized method for constructing

[a] School of Bio-Pharmaceutical Convergence, Hanyang University, Ansan 15588, Korea. E-mail: chanseok@hanyang.ac.kr
[b] Department of Mechanical Engineering, Seoul National University, Seoul 08826, Korea. E-mail: dnkim@snu.ac.kr
[c] Institute of Advanced Machines and Design, Seoul National University, Seoul 08826, Korea
[d] Institute of Engineering Research, Seoul National University, Seoul 08826, Korea
† Present address: Hanwha Aerospace R&D Center, Seongnam 13488, Korea.

This journal is © The Royal Society of Chemistry 2025

Published on 13 August 2025. Downloaded on 2/14/2026 1:29:38 AM.

DNA nanostructures with precise spatial control. Increased design flexibility by staple sequence design and high folding yield of this system led to the invention of various shape design tools from manual drawing to algorithm-based automated shape design tools,[20–24] enabling the construction of almost arbitrary geometries.

Currently, scaffolded DNA origami generally requires around 200 short staple strands, each 20–50 nt in length when M13mp18 ssDNA is used as a scaffold. The lower limit of staple length is to secure orthogonal binding to the programmed positions of the scaffold DNA, and its upper limit is an economical length range of solid phase synthesis of DNA oligos. Solid phase synthesis is a method that repeatedly adds nucleotide bases through stepwise chemical coupling reactions.[25] While this method is suitable for small-scale laboratory production of DNA nanostructures, it becomes cost-prohibitive and impractical for high-volume manufacturing, since the length and synthesis scale of oligonucleotides are inherently limited by cumulative error.[26] This limitation has prompted interest in alternative approaches that can integrate biotechnological synthesis.

Enzymatic production of DNA has attracted attention as a cost-effective method for manufacturing DNA assemblies.[4,27–32] Similar to the production of M13mp18 DNA from bacteriophage, bacterial synthesis based on the use of customized phagemid DNA carrying the desired sequence have enabled the large-scale production of staple strands.[30,33] However, the initial construction of the phagemid DNA, typically several kilobases in length, is complex, and modifying the sequence once the template is established is difficult. Also, the incorporation of modified bases is highly limited due to the constraints of *in vivo* replication fidelity. As a more accessible alternative for large-scale and functionalized DNA production, RCA offers a simpler and more flexible method. RCA is an *in vitro* amplification technique that generates long, repetitive single-stranded DNA products by using a DNA polymerase to continuously replicate a circular template. Although RCA has been explored for producing staple strands[4] or as a means to generate scaffold strands for DNA nanostructures,[34] the tandemly repeated nature of enzymatically synthesized DNA products poses challenges for conventional scaffolded DNA origami design.

In other words, while previous studies have explored the use of enzymatic production methods for large-scale production of DNA nanostructures, relatively little attention has been given to how DNA origami structures should be designed to take full advantage of such production strategies. In particular, producing numerous short DNA strands required in conventional DNA origami designs *via* enzymatic methods necessitates the repeated insertion of cleavage motifs into the template. For example, a 25-nt recognition site incorporating a hairpin motif was used for the BseGI restriction enzyme,[4] and the zinc ion-based self-excision mechanism requires approximately 87-nt.[30] These auxiliary sequences, which are comparable to or even longer than the staple strands themselves, must also be replicated along with the desired strands, resulting in significant inefficiency. This also increases the overall length and complexity of the template DNA. Therefore, to utilize enzymatically synthesized DNA more effectively in the production of DNA nanostructures, improved sequence design strategies are required.

In this study, we present a design framework that enables the use of long staple strands—around 100 to 200 nt in length—making them compatible with biologically scalable production methods such as bacterial synthesis and RCA. Our strategy aims to facilitate the generation of DNA nanostructures using enzymatically synthesized building blocks, thereby lowering production costs and enabling future integration with functional nucleotide modifications. While some studies have reported the construction of short bundle and brick-like structures with an average staple length of approximately 100 nt,[30,35] the applicability of longer staples across a wider range of design strategies has not yet been systematically explored. We demonstrate the applicability of this long-staple design across a range of DNA origami architectures, including the conventional rectangular sheet structure and six-helix bundle (6HB), as well as wireframe structures generated using automated shape design tools like PERDIX[23] and METIS.[24] In each case, we verified that replacing conventional short staples with long staples resulted in successful assembly and high structural integrity, indicating that our method is compatible with widely-used manual and automated DNA origami design approaches reported so far.

Furthermore, we established a biological production route to long staples using RCA by constructing circular DNA templates and employing enzymatic cleavage strategies. The resulting long staple strands were successfully incorporated into origami folding reactions, validating the feasibility of the overall workflow. This work lays the foundation for scalable production of DNA nanostructures and opens new possibilities for functional nanomaterial fabrication using modified nucleotides and enzymatic synthesis.

Results and discussion

Long-staple design for scaffolded DNA origami

To design scaffolded DNA origami more compatible with the enzymatic production of staple strands, we increased the length of constituting staples to reduce the number of templates and the repeating excision region in RCA products. The long-staple sequence design approach is broadly compatible with most scaffolded DNA origami architectures, including square- and hexagonal-lattice structures as well as lattice-independent wireframe geometries. This means that existing design frameworks for scaffolded DNA origami can be directly reused without major structural modifications. Importantly, the critical distinction lies not in the geometry of the structure, but in the method of strand organization—namely, the use of a long scaffold strand paired with complementary staple strands. As such, long-staple design is not compatible with architectures that rely on different assembly principles, such as tile-based assembly (which uses only short oligonucleotides)[36–38] or ssOrigami (which uses a single long strand without staples).[29]

Published on 13 August 2025. Downloaded on 2/14/2026 1:29:38 AM.

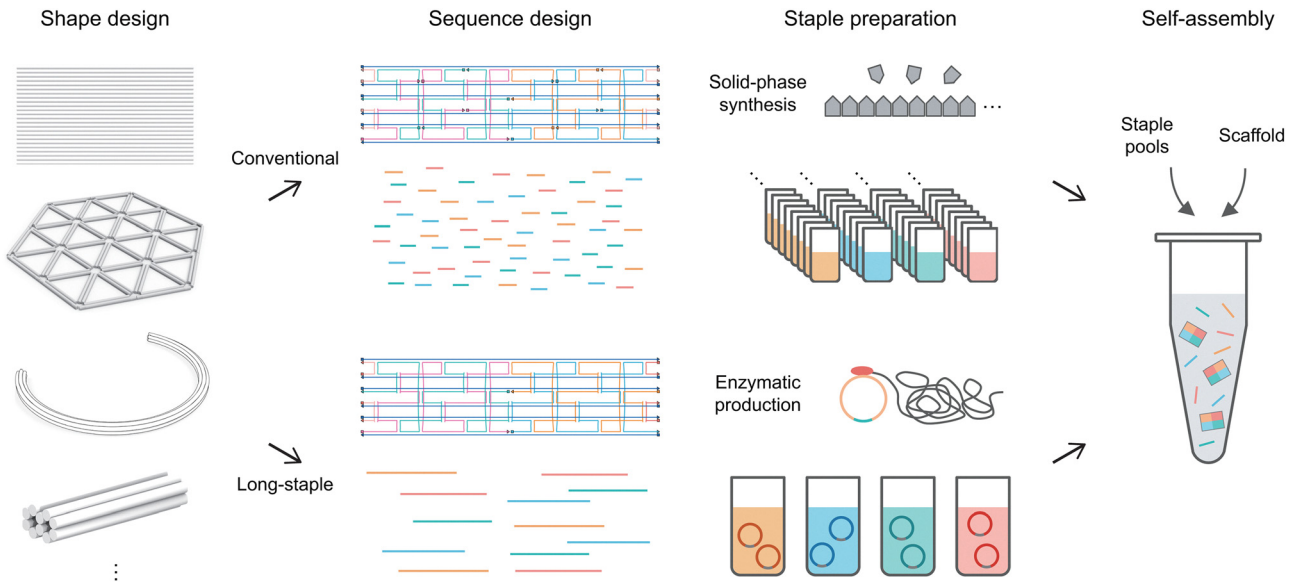

Fig. 1 Schematic illustration of long-staple design for enzymatic production of scaffolded DNA origami. By increasing the length and reducing the number of unique staple strands, the long-staple DNA design improves compatibility with biotechnological mass production methods such as rolling circle amplification (RCA), while remaining fully compatible with conventional scaffolded DNA origami design principles.

An overview of the long-staple origami design for scalable production is shown in Fig. 1. The design of long staples begins with modifying the output staple list from conventional design software by extending the lengths of adjacent staples to create longer, continuous sequences. This can be done either manually—by avoiding the use of automatic strand breaking functions such as the "autobreak" feature in caDNAno—or through custom scripts that define staple strand boundaries. Once the long staples are defined, a set of circular DNA templates need be prepared for RCA. This involves generating the reverse-complementary sequence of the full-length staple, and including a restriction site for subsequent cleavage. Since the RCA product consists of tandem repeats of sequences complementary to the template, suitable cleavage techniques such as the inclusion of restriction enzyme recognition sites[4] or DNAzyme sequence that cleave in the presence of Zn^{2+} ions are required.[30,33] In this study, we employed the restriction enzyme BtsCI, which recognizes a short cleavage sequence. This choice was made to keep the circular template length under 200 nt, enabling direct use of long oligonucleotide synthesis services available from commercial providers.

To complete template preparation, the linear oligonucleotide is circularized using a splint-assisted ligation step, followed by nick sealing with T4 DNA ligase. The circularized template is then used to initiate RCA with Phi29 DNA polymerase in the presence of dNTPs. The reaction can include single or multiple templates, allowing selective production of different long staples in a pooled reaction. This enables targeted modification of specific regions within the DNA nanostructure. Following amplification, the RCA products are enzymatically digested using a restriction enzyme to yield individual long staple strands. These strands can then be assembled into DNA nanostructures using standard thermal annealing protocols.

Validation of long-staple structures

We first applied the long-staple design strategy to a well-known rectangular structure (referred to as the "Rothemund square"). In the original design, 32 nt staple strands are used to form dsDNA and align them by connecting neighboring helices through crossovers with 32 bp intervals. In our modified design, 84 staple strands corresponding to 44% of the rectangle were replaced with longer staples (Fig. 2a).

In the case of 128-mer rectangle, we connected a series of four staple strands connected in tail-to-head. Agarose gel electrophoresis analysis of 128-mer rectangles assembled under different $MgCl_2$ concentrations and varying scaffold-to-staple ratios revealed that the optimal folding parameters (12–20 mM of magnesium and scaffold-to-staple ratio greater than 1 : 2) were comparable to those required for the conventional short-staple version (Fig. 2b and Fig. S1). AFM images of samples prepared with scaffold-to-staple ratios of 1 : 1 and 1 : 5 at 12 mM $MgCl_2$ showed that, under 1 : 1 stoichiometry, some structures were partially broken and failed to form clear rectangular shapes as intended (Fig. 2c).

We further lengthened the staple strands up to 192 nt by connecting six consecutively linked staples (Fig. 2d). Both the optimal range of parameters and resulting structural integrity were consistent with those of the short and 128-mer rectangle (Fig. 2e, f, and Fig. S1). These results indicate that, in constructing scaffolded DNA nanostructures, staple strands do not necessarily need to fall within the conventional length range (20 nt to 50 nt); even substantially longer staples can be used without compromising the folding yield and structural quality. Even with the introduction of long staples, the lengths of scaffold segments between crossover points ("seed" length[39]) remain unchanged, suggesting that the self-assembly parameters are likely to be similar.

 This journal is © The Royal Society of Chemistry 2025

Published on 13 August 2025. Downloaded on 2/14/2026 1:29:38 AM.

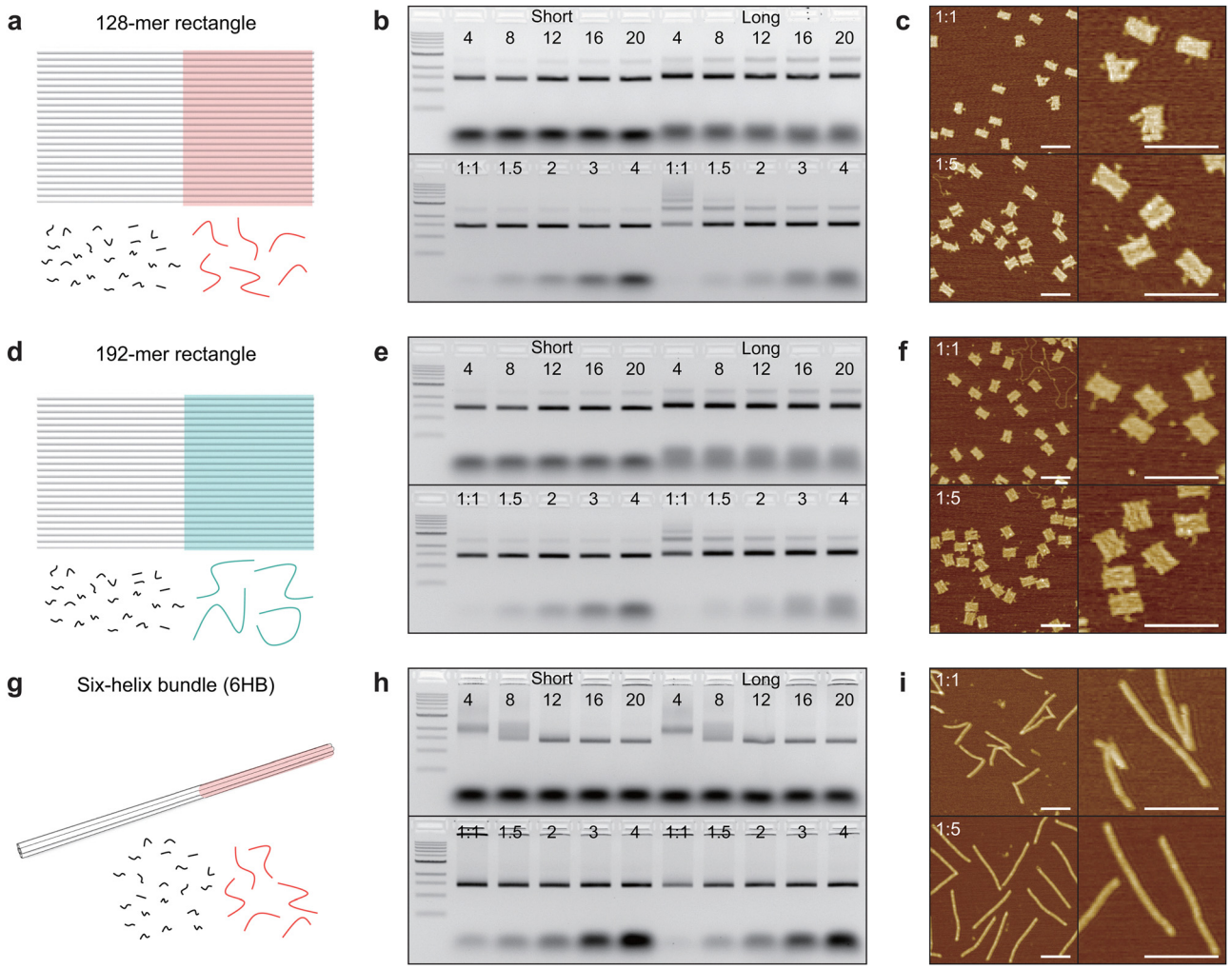

Fig. 2 Assessment of long-staple design for planar and hexagonal lattice DNA origami structures. (a) Schematic illustration of a rectangular DNA origami structure partially comprising 128-mer-long staple strands. (b) Agarose gel electrophoresis results of DNA origami rectangles assembled with short or 128-mer-long staples under varying folding conditions. Upper gel: variation of magnesium ion concentration under same scaffold-staple ratio of 1 : 5. Lower gel: variation of scaffold-to-staple ratios under 12 mM $MgCl_2$. (c) Representative AFM images of samples prepared with scaffold-to-staple ratios of 1 : 1 and 1 : 5 at 12 mM $MgCl_2$, respectively. Scale bars are 200 nm. More images are provided in Fig. S1. (d) Schematic illustration of a rectangular DNA origami structure partially comprising 192-mer-long staple strands. (e) Agarose gel electrophoresis results of DNA origami rectangles assembled with short or 192-mer-long staples under varying folding conditions. Upper gel: variation of magnesium ion concentration under same scaffold-staple ratio of 1 : 5. Lower gel: variation of scaffold-to-staple ratios under 12 mM $MgCl_2$. (f) Representative AFM images of samples prepared with scaffold-to-staple ratios of 1 : 1 and 1 : 4 at 12 mM $MgCl_2$, respectively. Scale bars are 200 nm. More images are provided in Fig. S1. (g) Schematic illustration of a six-helix bundle DNA origami structure partially comprising 126-mer-long staple strands. (h) Agarose gel electrophoresis results of 6HB DNA origami assembled with short or 126-mer-long staples under varying folding conditions. Upper gel: variation of magnesium ion concentration at the same scaffold-staple ratio of 1 : 5. Lower gel: variation of scaffold-to-staple ratios with 16 mM $MgCl_2$. (i) Representative AFM images of samples prepared with scaffold-to-staple ratios of 1 : 1 and 1 : 5 at 16 mM $MgCl_2$, respectively. More images are provided in Fig. S2. Scale bars are 200 nm.

To further explore the feasibility of longer staples to three-dimensional structures, we also tested a six-helix-bundle (6HB) structure with short (42 nt) and long (126 nt) staple versions (Fig. 2g). Similar to previous results, long staple structures were well folded under similar assembly conditions (Fig. 2h and Fig. S2). Here, AFM images show that structures with a low scaffold-to-staple ratio showed many kinked structures (Fig. 2i). From the results, it was found that rather than the staple strand length itself, the stoichiometric ratio between the scaffold and staple DNA plays a far more critical role in determining the assembly yield of DNA nanostructures.

The previous results were obtained using structures in which a specific region of the full DNA origami was substituted with long staples, while the remainder was assembled using conventional short staples. To further validate the feasibility of the long-staple design strategy, we constructed structures consisting exclusively of either short or long staples within the same region. Both designs yielded identical gel electrophoresis patterns (Fig. S3). These results confirm that the long-staple design is compatible with both small DNA origami structures that do not utilize the entire scaffold and hybrid designs that incorporate a mixture of long and short staples.

Published on 13 August 2025. Downloaded on 2/14/2026 1:29:38 AM.

Feasibility of long-staple design for wireframe-based designs

Next, we applied the long-staple approach to other designs, to validate its compatibility with conventional automated shape design tools. We used PERDIX,[23] a design program for two-dimensional wireframe structures, in which edges are composed of two-helix bundles with antiparallel double crossover (DX) motifs, and vertices are formed by multi-arm junctions. To make long-staple design from the exported sequence list, we connected all staples constituting each edge, and as well as staples forming multi-arm junctions. First, a miniaturized hexagonal structure with six small triangles, each with an edge length of 105 bp, was designed using 37% of scaffold length (2689 out of 7249 nt) (Fig. 3a). The unpaired regions of the scaffold DNA dangle from the assembled structure. The original (short) version of this structure consists of 63 staple strands (48 edge staples and 15 vertex staples) whose lengths range from 37 nt to 56 nt. In the modified long-staple structure, each duplex edge and multi-arm junction was constructed using a long staple strand, therefore 19 staples (12 for edges and 7 for vertices) were used whose lengths are either 98 nt or 168 nt. In the process of long-staple design, the number of inter-helix crossovers connecting the adjacent DNA helix along each edge is reduced. While this could potentially introduce structural instability, we considered that it would not pose a significant issue, as wireframe-based designs typically feature edge lengths shorter than the persistence length of double-stranded DNA (~150 bp).

SNUPI simulations were performed to assess the structural stability of the wireframe assemblies consisting of short and long staples. Both staple designs yielded predicted structures matching the intended geometry, with negligible differences between the two (Fig. 3a, d, g and Fig. S4). In SNUPI modeling, all complementary base pairings between scaffold and staples are assumed to be fully hybridized, and the mechanical properties of base-pair steps containing a nick (single-stranded break)

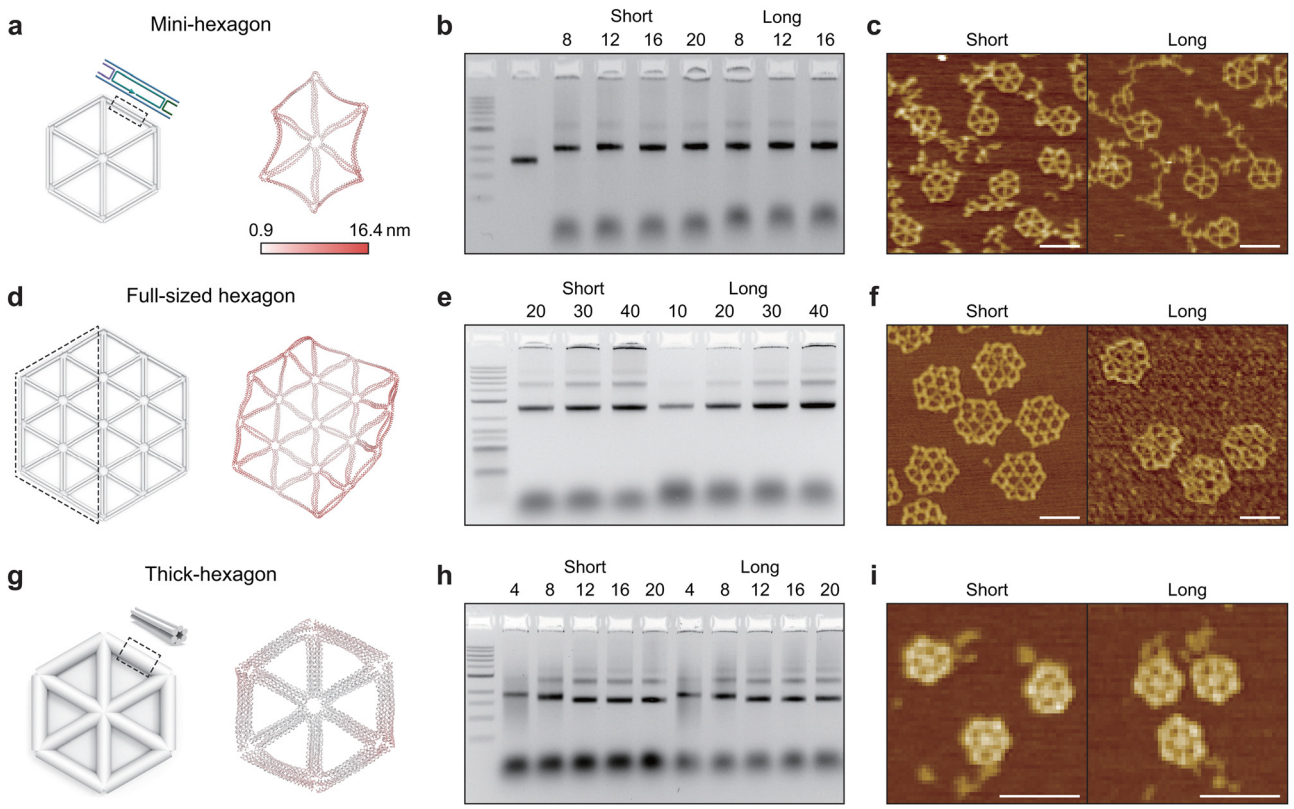

Fig. 3 Application of long-staple design to wireframe-based DNA origami architectures. (a) Schematic illustration and SNUPI simulation result of a miniaturized hexagonal structure designed using PERDIX. Colors in the rendering on the right panel represent the root-mean-square fluctuation (RMSF) of each node; SNUPI results in (d) and (g) are mapped using the same scale. More simulation results are provided in Fig. S4. (b) Agarose gel electrophoresis result of short- and long-staple version of mini hexagons assembled at different Mg^{2+} concentrations. (c) Representative AFM images of short- and long-staple versions of mini hexagons prepared with scaffold-to-staple ratios of 1 : 5 and 12 mM $MgCl_2$, respectively. More images are provided in Fig. S4. (d) Schematic illustration of a full-sized hexagonal structure and SNUPI simulation result. In the long-staple version of the design, the region enclosed by the dashed lines was replaced with long staples. (e) Agarose gel electrophoresis result of short- and long-staple version of full-sized hexagons assembled under 12 mM $MgCl_2$ with different scaffold concentrations. Final concentration of each staple strand was fixed as 100 nM. (f) Representative AFM images of short- and long-staple versions of full-sized hexagons prepared with scaffold-to-staple ratios of 1 : 5 and 12 mM $MgCl_2$, respectively. More images are provided in Fig. S5. (g) Schematic illustration and SNUPI simulation result of a thick hexagonal structure designed using METIS. (h) Agarose gel electrophoresis result of short- and long-staple version of thick hexagons assembled under different Mg^{2+} concentrations. (i) Representative AFM images of short- and long-staple versions of thick hexagons prepared with scaffold-to-staple ratios of 1 : 5 and 16 mM $MgCl_2$, respectively. More images are provided in Fig. S6. Scale bars are 100 nm.

 This journal is © The Royal Society of Chemistry 2025

Published on 13 August 2025. Downloaded on 2/14/2026 1:29:38 AM.

are similar to those of regular base-pair steps.[8] In other words, although the number of DNA nicks is reduced in the long-staple design, this has negligible impact on the overall shape or flexibility of the resulting structure. In accordance with the simulation results, both the short- and long-staple versions of the structure exhibited nearly identical migration distances in agarose gel electrophoresis, as well as similar individual morphologies in AFM images (Fig. 3b, c and Fig. S5). These results confirm that the long-staple design strategy is also applicable to wireframe-based DNA nanostructures.

Building on the successive assembly of the miniaturized design, we extend the approach to a full scaffold (Fig. 3d). Here, the 'short' version has 177 staples (126 for edges and 51 for vertices). In the case of 'long' design, approximately half of the structure was constructed using 26 long staples (19 for edges and 7 for vertices) that have 98-mer to 162-mer length. Under the optimal concentration of $MgCl_2$, both long and short design structures assembled well across different scaffold concentrations (Fig. 3e). Also, both versions showed similar structural characteristics without notable defects (Fig. 3f and Fig. S5). We have observed slight distortion of the structures in the AFM image, due to the high flexibility of the design as predicted *via* SNUPI analysis.

We tested another automated design program, METIS.[24] It generates similar 2D wireframe structures like PERDIX, but it uses hexagonal 6HB as edges and multiway vertex motifs to reinforce the structural rigidity. The METIS hexagon structure has six small triangles with 84-bp-long edges and possesses 5645 nt of the scaffold. The unpaired region of the scaffold (approx. 1600 nt) was dangled to the structure. For the long-staple version, 23 long edge staples (93 nt to 168 nt) were used instead of 64 short edge staples, and 25 long vertex staples (85 nt to 164 nt) replaced 62 short vertex staples. Again, both short and long version of the structures were well-folded as validated by gel electrophoresis and AFM imaging (Fig. 3h, i, and Fig. S6).

Long-staple production using RCA

Through the series of experiments described above, we confirmed that the long-staple design is well compatible with commonly used design strategies in scaffolded DNA origami. Based on this result, we demonstrated a biotechnological production workflow to generate long staple strands using

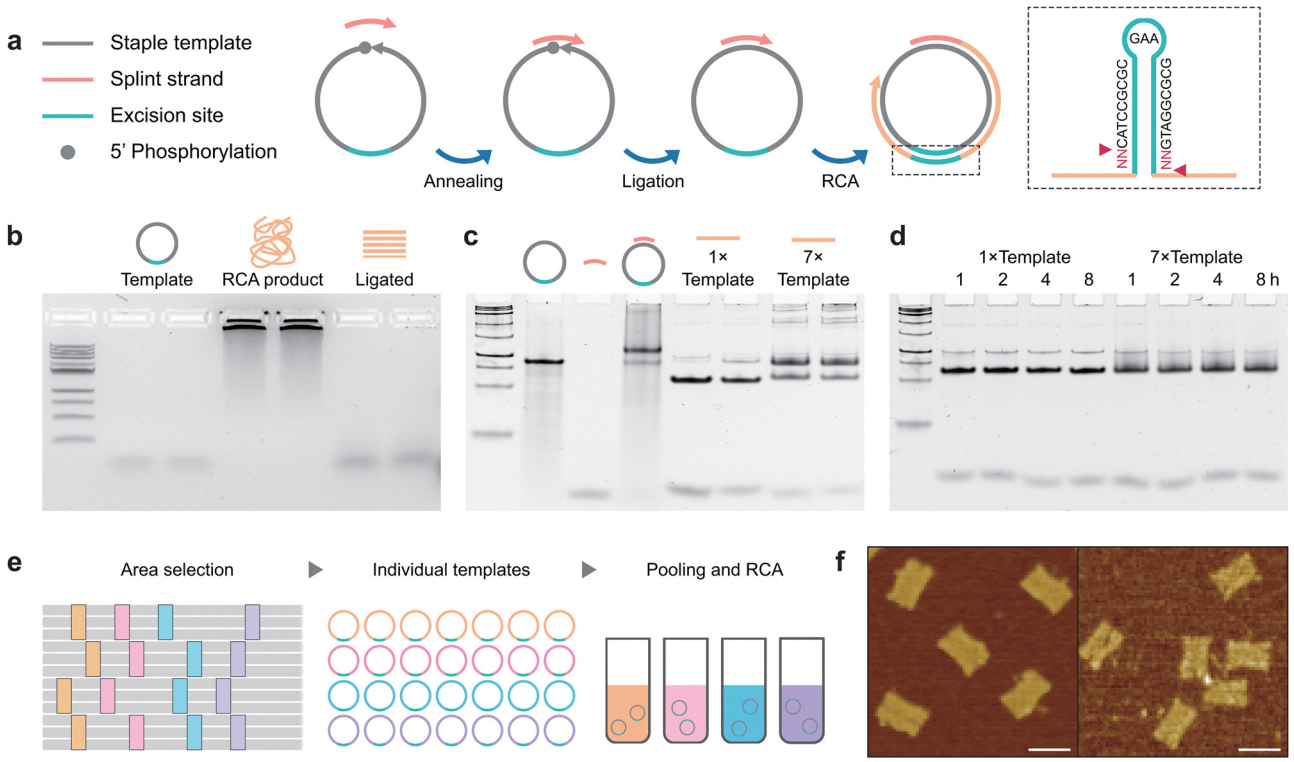

Fig. 4 Enzymatic production of long staples. (a) Schematic illustration of the design, circularization, and ligation process for producing a circular RCA template. Arrowheads indicate the 3′ end of DNA strands. The boxed region shows an enlarged view of the hairpin element designed for restriction enzyme cleavage. The red triangles indicate DNA cleavage sites. "NN" denotes arbitrary nucleotides. (b) Agarose gel image showing two different circular templates, their corresponding RCA products, and the resulting strands after restriction enzyme digestion. (c) PAGE image showing the circular template preparation and cleavage efficiency of RCA products. Templates containing a TA hairpin sequence near the BtsCI cleavage site were used. Templates were used either individually or as a pool of seven distinct sequences. RCA products (1.5 or 3 μg) were incubated with BtsCI for 8 hours, revealing that pooling multiple templates leads to reduced cleavage efficiency. (d) PAGE image showing improved cleavage results when the hairpin sequence adjacent to the cleavage site was changed to AA. Even under pooled template conditions, RCA products (1.5 μg) were more effectively cleaved with shorter incubation times. (e) Schematics showing the procedure for assembling part of a rectangular origami structure using RCA-generated long staples. (f) AFM images of structures assembled with short staples (left) and with a mixture of short and RCA-derived long staples (right). Scale bars are 100 nm.

Published on 13 August 2025. Downloaded on 2/14/2026 1:29:38 AM.

RCA (Fig. 4a). In contrast to previous approaches,[4,30] we designed a unique circular template for each long staple strand. This was done to allow easy ordering of template DNA *via* oligonucleotide synthesis services rather than full gene synthesis, and to enable a modular production system in which individual staple strands can be synthesized separately or pooled together for parallel production. Each circular template was designed to be reverse-complementary to the original staple sequence. Due to the tandem repeat nature of RCA products, we adopted a restriction site for the enzyme BseGI to facilitate the recovery of discrete staple strands. BseGI recognizes the 5′-GGATG-3′ sequence on double-stranded DNA and cleaves at this site. To create the necessary dsDNA region for cleavage, a short hairpin structure was incorporated into the template design.[4] A portion of the staple sequence itself was also used as a splint strand to circularize the linear DNA, and a 5′-phosphorylation was added to enable ligation using the T4 DNA ligase.

The RCA experiments successfully produced long staple strands from their corresponding circular templates using Phi29 polymerase, and individual staple strands were recovered through enzymatic digestion using BseGI (Fig. 4b). We further optimized both the RCA and digestion steps to improve production efficiency. PAGE analysis revealed that digestion efficiency was reduced when multiple templates were pooled into a single RCA reaction (Fig. 4c). Referring to previous studies indicating that flanking sequences can influence BseGI activity,[40] we redesigned the bases adjacent to the restriction site in the hairpin to include a ''AA'' sequence, which resulted in improved cleavage efficiency (Fig. 4d).

Based on the results, we redesigned part of the rectangular DNA origami structure using 28 long staples, and produced them by RCA. It was confirmed through AFM imaging that the assembled structure retained a well-defined rectangular shape, comparable to that achieved with conventional solid-phase synthesized long staples (Fig. 4e and f).

Conclusions

In this study, we proposed and validated a long-staple design strategy for scaffolded DNA origami that reduces the number of staple strands by extending their lengths to 100–200 nt. This approach was shown to be compatible with a wide range of origami architectures—including planar, bundle, and wireframe structures—generated by both manual and algorithmic design tools. Across all tested designs, structures assembled with long staples exhibited folding behavior and morphology comparable to those assembled using conventional short staples, demonstrating that the core principles of DNA origami self-assembly remain effective with longer strand designs.

To facilitate scalable production, we implemented a RCA-based workflow using individually designed circular templates for each long staple. The modular nature of this system allows for flexible, selective synthesis of specific staples, either independently or in pooled reactions. Integrating the long staple design concept into existing DNA origami design software, along with implementing an algorithm that automatically generates the corresponding template sequences for enzymatic production, is expected to greatly enhance the practical utility of this approach.

Although we did not construct entire structures solely with RCA-derived long staples, these staples were successfully incorporated into rectangular origami structures, confirming the practical feasibility of enzymatic production. To achieve full-scale enzymatic production of DNA origami, further studies will be required to determine the number of long staples that can be produced from a single RCA pool and to optimize various experimental parameters throughout the RCA production process. Nonetheless, this modular production approach is expected to facilitate sequence-level customization and functionalization of staple strands, offering greater flexibility in structural design and downstream applications.

Considering the inherent characteristics of scaffolded DNA origami, where numerous different sequence combinations can give rise to the same target structure, the long-staple design approach necessitates more precise sequence-level optimization for a given structure. Although the long-staple approach can reliably produce DNA nanostructures by leveraging the broad applicability of scaffolded DNA origami and well-established shape design principles, achieving higher yields and more sophisticated structures with longer staples is likely to require optimization at the nucleotide sequence level. Furthermore, the enzymatic cleavage techniques commonly used to cut long RCA-derived strands present a cost-related drawback. Thus, the development of more efficient and cost-effective cleavage methods will likely be necessary to further advance the practical utility of this approach. While RCA was used as the demonstration platform in this study, the same design principles are readily applicable to bacterial-based DNA synthesis methods.

Overall, the long-staple strategy offers a structurally robust and scalable approach to DNA origami fabrication and opens the door to integrating biologically synthesized or chemically modified nucleotides. This framework is expected to be used for future applications that require cost-effective, customizable, and functional DNA nanostructures.

Experimental

Sequence design and DNA origami assembly

The rectangular and 6HB structures were designed using caDNAno.[41] The small- and full-sized hexagon structures were designed using PERDIX, and the thick hexagon was generated using METIS. Following the initial structure design, long-staple sequences were manually arranged in caDNAno. Sequences of all staple strands used in this study are summarized in Tables S1–S6. As a scaffold, the M13mp18 single-stranded DNA (7249 nt; Guild BioSciences, USA) was used for all structures except the full-sized hexagon, which was assembled using a 7560-nucleotide scaffold from the same vendor. Typical short staples

 This journal is © The Royal Society of Chemistry 2025

Published on 13 August 2025. Downloaded on 2/14/2026 1:29:38 AM.

were provided by Bioneer and Bionics (Korea). Long staple strands were synthesized using Ultramer DNA oligonucleotide synthesis (IDT, USA) and Extendamer service (Bioneer, Korea). These long staples were diluted and mixed with short staple strands at equimolar concentrations.

For the general self-assembly process, a 100 μL folding mixture was prepared containing scaffold DNA (20 nM), staple strand (100 nM each), 1× TAE buffer (40 mM Tris-acetate and 1 mM EDTA), and $MgCl_2$ (12–20 mM). The final mixture was subjected to a self-assembly process using a thermocycler (T100; Bio-Rad, USA) under the following temperature profile: heating to 80 °C at a rate of 1 °C per s; cooling down from 80 °C to 65 °C over 1 h (−0.5 °C every 2 min) and gradual cooling from 65 °C to 25 °C over 40 h (−0.5 °C every 30 min); and held at 4 °C. After self-assembly, excessive nucleic acid strands were removed by centrifugal filtration using Amicon Ultra centrifugal filter units with 50 kDa molecular weight cut-off (UFC505096; Merck KGaA, USA).

AFM measurement

Assembled DNA origami structures were diluted with the annealing buffer to approximately 0.5–1 nM prior to the measurement. The prepared sample (20 μL) was deposited on a freshly cleaved mica substrate (highest grade V1 AFM Mica; Ted-Pella Inc., USA) and subsequently incubated for 5 min. The substrate was washed with DI water three times and gently dried using a N_2 gun (<0.1 kgf cm^{-2}). AFM images were obtained using NX10 (Park Systems, Korea) and a PPP-NCHR probe with a spring constant of 42 N m^{-1} (Nanosensors, Switzerland). The non-contact mode was used to measure typically 5 μm × 5 μm of the sample area at 1024 × 1024 pixel resolution using the SmartScan software. All measured images were flattened in linear and quadratic order using the XEI 4.1.0 program (Park Systems).

Agarose gel electrophoresis

Samples were electrophoresed on 1.5% agarose gels containing 0.5× TBE and 12 mM $MgCl_2$. The loaded samples were allowed to migrate for 1.5 h at 75 V bias voltage (approximately 3.7 V cm^{-1}) in an ice-water cooled chamber (Wide Mini-Sub Cell; Bio-Rad, USA). The gels were stained using 0.5 μg mL^{-1} ethidium bromide (EtBr) solution (Noble Bioscience Inc., Korea), and imaging was performed using the GelDoc XR+ device and the Image Lab v5.1 program (Bio-Rad).

Production of long staples using the RCA process

Linear RCA template strands were synthesized by IDT Ultramer DNA oligonucleotide synthesis service with 5′ phosphorylation. For the circularization process, the template and splint strands were mixed at equimolar concentrations (2 μM each) and subjected to a thermal annealing process by cooling from 85 °C to 25 °C over 100 min in 1× TE buffer containing 100 mM NaCl. Ligation was carried out by adding the T4 DNA ligase to the annealed mixture, followed by incubation at room temperature for 3 h and subsequent heat treatment at 70 °C for 20 min to terminate the reaction. For the RCA process, the circular template was incubated at 30 °C for up to 20 h under the following conditions: 0.05 μM circular template, 0.2 U μL^{-1} Phi29 DNA polymerase (Thermo Fisher Scientific, USA), 1× polymerase buffer, 5 mM dNTP mix, and 0.1 U μL^{-1} pyrophosphatase. The reaction was terminated by heating the mixture at 80 °C for 10 min to inactivate the enzymes. The uniformly dissolved RCA product was spun down 15 000 × *g* for 10 min with a 30 kDa cutoff Amicon filter (Merck Millipore) to acquire a concentrated stock solution. The concentrations of solutions were measured using a NanoDrop spectrophotometer (Thermo Fisher Scientific, USA). For BtsCI digestion, 1.5 μg of RCA product was incubated with 20 U of BtsCI in 1× rCutSmart™ Buffer (New England Biolabs, USA) at 37 °C for up to 8 hours.

Polyacrylamide gel electrophoresis (PAGE)

Polyacrylamide gel was cast by mixing 6 mL of 40% acrylamide/bis-acrylamide solution (19 : 1 ratio), 400 μL of 50× TAE buffer, 13.6 μL of DI water, 120 μL of 10% (w/v) ammonium persulfate solution, and 12 μL of tetramethylethylenediamine (TEMED). Gels were mounted on a Mini-Protean Tetra Cell (Bio-Rad) filled with 1× TAE buffer, and 1 μL of each sample mixed with gel loading dye purple (B7024S, New England BioLabs) was loaded onto the gel. After running the gels at 100 V for 70 min, they were stained with SYBR gold solution for 10 min. Gel imaging was performed using a Gel Doc XR+ documentation system (Bio-Rad).

Author contributions

C. L. and D.-N. K. conceived and supervised the project. C. L., Y. K., and K. J. designed and performed the experiments. C. L. analyzed the experimental data. T. R. performed computational analysis of the structures. C. L. and D.-N. K. wrote the manuscript. All authors reviewed and revised the manuscript.

Conflicts of interest

There are no conflicts to declare.

Data availability

The data that support the findings of this study are included in the main text and the SI. More data are available from the corresponding author upon reasonable request. Requests for further information, resources, and reagents should be directed to and will be fulfilled by the lead contact, Do-Nyun Kim.

Additional AFM images of all structures, agarose gel electrophoresis results for partially assembled structures, more detailed SNUPI simulation data, and the sequences of all staple strands used in the experiments. See DOI: **https://doi.org/10.1039/d5nh00357a**

Published on 13 August 2025. Downloaded on 2/14/2026 1:29:38 AM.

Acknowledgements

This work was supported by the National Research Foundation of Korea (NRF) grant funded by the Korean government (MSIT) (RS-2021-NR061805, RS-2024-00346176), the grant of the Korea-US Collaborative Research Fund (KUCRF), funded by the Ministry of Science and ICT and Ministry of Health & Welfare, Republic of Korea (RS-2024-00468463), and the research fund of Hanyang University (HY-2024-0497).

References

1 N. C. Seeman, *J. Theor. Biol.*, 1982, **99**, 237–247.
2 S. Dey, C. Fan, K. V. Gothelf, J. Li, C. Lin, L. Liu, N. Liu, M. A. D. Nijenhuis, B. Saccà, F. C. Simmel, H. Yan and P. Zhan, *Nat. Rev. Methods Primers*, 2021, **1**, 13.
3 P. W. K. Rothemund, *Nature*, 2006, **440**, 297–302.
4 C. Ducani, C. Kaul, M. Moche, W. M. Shih and B. Högberg, *Nat. Methods*, 2013, **10**, 647–652.
5 D.-N. Kim, F. Kilchherr, H. Dietz and M. Bathe, *Nucleic Acids Res.*, 2012, **40**, 2862–2868.
6 J. P. K. Doye, T. E. Ouldridge, A. A. Louis, F. Romano, P. Šulc, C. Matek, B. E. K. Snodin, L. Rovigatti, J. S. Schreck, R. M. Harrison and W. P. J. Smith, *Phys. Chem. Chem. Phys.*, 2013, **15**, 20395–20414.
7 C. Maffeo and A. Aksimentiev, *Nucleic Acids Res.*, 2020, **48**, 5135–5146.
8 J. Y. Lee, J. G. Lee, G. Yun, C. Lee, Y.-J. Kim, K. S. Kim, T. H. Kim and D.-N. Kim, *ACS Nano*, 2021, **15**, 1002–1015.
9 C. E. Castro, F. Kilchherr, D.-N. Kim, E. L. Shiao, T. Wauer, P. Wortmann, M. Bathe and H. Dietz, *Nat. Methods*, 2011, **8**, 221–229.
10 K. Xia, J. Shen, Q. Li, C. Fan and H. Gu, *ACS Nano*, 2020, **14**, 1319–1337.
11 F. Hong, F. Zhang, Y. Liu and H. Yan, *Chem. Rev.*, 2017, **117**, 12584–12640.
12 W. Engelen and H. Dietz, *Annu. Rev. Biophys.*, 2021, **50**, 469–492.
13 M. Kim, C. Lee, K. Jeon, J. Y. Lee, Y.-J. Kim, J. G. Lee, H. Kim, M. Cho and D.-N. Kim, *Nature*, 2023, **619**, 78–86.
14 M. Xiao, W. Lai, T. Man, B. Chang, L. Li, A. R. Chandrasekaran and H. Pei, *Chem. Rev.*, 2019, **119**, 11631–11717.
15 Y. Wang, C. Shen, C. Wu, Z. Zhan, R. Qu, Y. Xie and P. Chen, *Research*, 2024, **7**, 0352.
16 S. Li, Q. Jiang, S. Liu, Y. Zhang, Y. Tian, C. Song, J. Wang, Y. Zou, G. J. Anderson, J.-Y. Han, Y. Chang, Y. Liu, C. Zhang, L. Chen, G. Zhou, G. Nie, H. Yan, B. Ding and Y. Zhao, *Nat. Biotechnol.*, 2018, **36**, 258–264.
17 M. Komiyama, N. Shigi and K. Ariga, *Adv. Funct. Mater.*, 2022, **32**, 2200924.
18 L. Li, J. Yin, W. Ma, L. Tang, J. Zou, L. Yang, T. Du, Y. Zhao, L. Wang, Z. Yang, C. Fan, J. Chao and X. Chen, *Nat. Mater.*, 2024, **23**, 993–1001.
19 Y. C. Zeng, O. J. Young, C. M. Wintersinger, F. M. Anastassacos, J. I. MacDonald, G. Isinelli, M. O. Dellacherie, M. Sobral, H. Bai, A. R. Graveline, A. Vernet, M. Sanchez, K. Mulligan, Y. Choi, T. C. Ferrante, D. B. Keskin, G. G. Fell, D. Neuberg, C. J. Wu, D. J. Mooney, I. C. Kwon, J. H. Ryu and W. M. Shih, *Nat. Nanotechnol.*, 2024, **19**, 1055–1065.
20 S. M. Douglas, H. Dietz, T. Liedl, B. Hogberg, F. Graf and W. M. Shih, *Nature*, 2009, **459**, 414–418.
21 E. Benson, A. Mohammed, J. Gardell, S. Masich, E. Czeizler, P. Orponen and B. Högberg, *Nature*, 2015, **523**, 441–444.
22 R. Veneziano, S. Ratanalert, K. Zhang, F. Zhang, H. Yan, W. Chiu and M. Bathe, *Science*, 2016, **352**, 1534.
23 H. Jun, F. Zhang, T. Shepherd, S. Ratanalert, X. Qi, H. Yan and M. Bathe, *Sci. Adv.*, 2019, **5**, eaav0655.
24 H. Jun, X. Wang, W. P. Bricker and M. Bathe, *Nat. Commun.*, 2019, **10**, 5419.
25 M. H. Caruthers, *Science*, 1985, **230**, 281–285.
26 S. Kosuri and G. M. Church, *Nat. Methods*, 2014, **11**, 499–507.
27 R. Veneziano, T. R. Shepherd, S. Ratanalert, L. Bellou, C. Tao and M. Bathe, *Sci. Rep.*, 2018, **8**, 6548.
28 M. Xu, C. Zhang, C. Zhang, Y. Zhao, Z. Qi, C. Fan, J. Chao and B. Wei, *ACS Mater. Lett.*, 2020, **2**, 1322–1327.
29 D. Han, X. Qi, C. Myhrvold, B. Wang, M. Dai, S. Jiang, M. Bates, Y. Liu, B. An, F. Zhang, H. Yan and P. Yin, *Science*, 2017, **358**, eaao2648.
30 F. Praetorius, B. Kick, K. L. Behler, M. N. Honemann, D. Weuster-Botz and H. Dietz, *Nature*, 2017, **552**, 84–87.
31 B. Kick, F. Praetorius, H. Dietz and D. Weuster-Botz, *Nano Lett.*, 2015, **15**, 4672–4676.
32 X. Chen, Q. Wang, J. Peng, Q. Long, H. Yu and Z. Li, *ACS Appl. Mater. Interfaces*, 2018, **10**, 24344–24348.
33 F. A. S. Engelhardt, F. Praetorius, C. H. Wachauf, G. Brüggenthies, F. Kohler, B. Kick, K. L. Kadletz, P. N. Pham, K. L. Behler, T. Gerling and H. Dietz, *ACS Nano*, 2019, **13**, 5015–5027.
34 Y. Ma, H. Zheng, C. Wang, Q. Yan, J. Chao, C. Fan and S.-J. Xiao, *J. Am. Chem. Soc.*, 2013, **135**, 2959–2962.
35 S. Niekamp, K. Blumer, P. M. Nafisi, K. Tsui, J. Garbutt and S. M. Douglas, *Nucleic Acids Res.*, 2016, **44**, e102.
36 P. Yin, R. F. Hariadi, S. Sahu, H. M. T. Choi, S. H. Park, T. H. LaBean and J. H. Reif, *Science*, 2008, **321**, 824–826.
37 Y. Ke, L. L. Ong, W. M. Shih and P. Yin, *Science*, 2012, **338**, 1177–1183.
38 B. Wei, M. Dai and P. Yin, *Nature*, 2012, **485**, 623–626.
39 T. G. Martin and H. Dietz, *Nat. Commun.*, 2012, **3**, 1103.
40 J. Rosa, E. Fernandez-Gonzalez, C. Ducani and B. Högberg, *PLoS One*, 2018, **13**, e0202057.
41 S. M. Douglas, A. H. Marblestone, S. Teerapittayanon, A. Vazquez, G. M. Church and W. M. Shih, *Nucleic Acids Res.*, 2009, **37**, 5001–5006.

 This journal is © The Royal Society of Chemistry 2025